This is a repository copy of *Spectroscopy 2050 – The Future of Ultrafast 2D-IR Spectroscopy*.

White Rose Research Online URL for this paper:
https://eprints.whiterose.ac.uk/213662/

Version: Accepted Version

Article:

Spectroscopy 2050 – The Future of Ultrafast 2D-IR Spectroscopy

Amy L. Farmer, Kelly Brown, Neil T. Hunt*

Department of Chemistry and York Biomedical Research Institute, University of York, York, UK

* Corresponding author: neil.hunt@york.ac.uk

Abstract

The intention of this review is to reflect on the development of ultrafast 2D-IR spectroscopy to date and to attempt to envisage how the technique might develop in the period between now and 2050. As ultrafast 2D-IR spectroscopy measurements were first-reported in 1998, the timing of this article represents a 'halfway' stage, allowing us to look back on 26 years of development to provide a perspective on what the next 26 years might bring. We begin by briefly introducing the method and summarising the development of 2D-IR experiments thus far, but then focus on the most recent advances in technology, sample handling and data analysis methods to inform a discussion on the direction of travel for the field in terms of measurement capabilities. Finally, we examine the most recent applications of 2D-IR, with a particular focus on emerging research areas to show how the field continues to explore new challenges and provide novel insights.

Introduction to the 2D-IR method and historical context

Infrared (IR) absorption spectroscopy is a commonly-employed technique that has been used to provide molecular insight across a broad range of chemical and biomolecular applications. By measuring the specific frequencies or wavelengths at which molecules absorb IR radiation, detailed information can be obtained regarding the vibrational energy levels, bonding, symmetry and structure of a molecule, while lineshapes report on dynamic phenomena such as lifetimes and the impact of intermolecular interactions. However, in the case of samples with complex spectra or where significant line-broadening occurs, this information can be hard to extract from a one-dimensional spectrum, while information on dynamic timescales is lost when using normal absorption spectroscopy approaches.

The relationship between ultrafast two-dimensional infrared (2D-IR) spectroscopy and IR absorption is broadly analogous to that between one and two-dimensional NMR experiments. 2D-IR measurements introduce a second frequency dimension to the IR spectrum such that the bands found in an IR absorption (frequently referred to as FT-IR) spectrum appear on the diagonal of the 2D-plot, while off-diagonal peaks appear that provide new information relating to vibrational mode coupling, structure and energy transfer processes.[1-3] The 2D-representation of the molecular IR response also brings benefits in terms of reduced spectral congestion.

The ability to access this additional information arises because the 2D-IR signal is generated by sequence of IR laser pulses which first excite (pump) the vibrational modes of the sample and then follow (probe) the impact of the excitation on other modes (Fig. 1(a)). Formally, this is a 3rd order non-linear spectroscopy technique, which leads to a 2D plot that is a correlation map of excitation (pump)
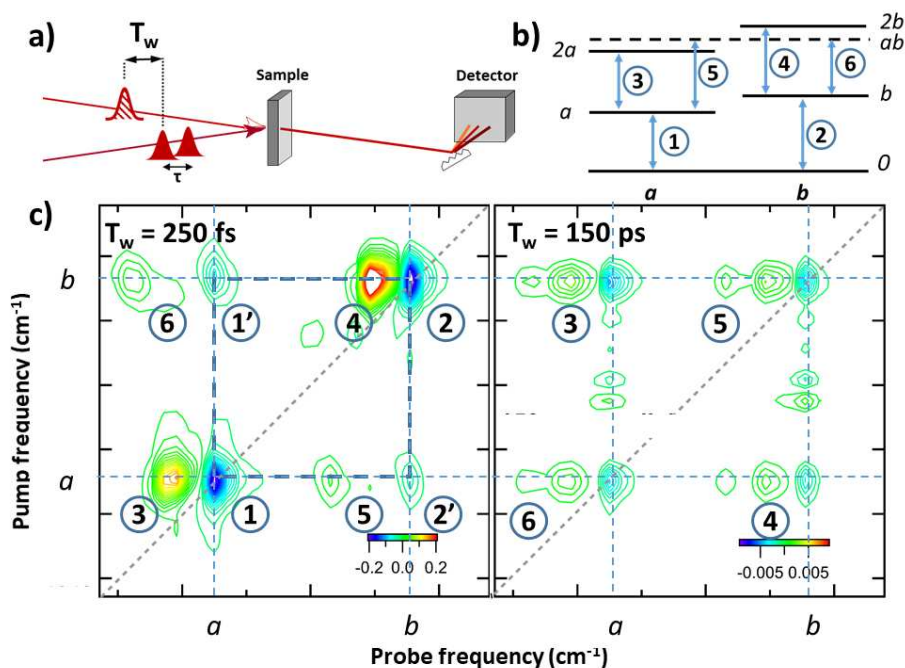
Figure 1: *Schematic introduction to 2D-IR spectroscopy. a) Diagram of experimental arrangement showing two pump (solid red) and one probe pulse (hatched) used to generate the 2D-IR signal and the waiting time T_w. B) Energy level diagram of a simple set of two coupled vibrational modes discussed in the text. c) 2D-IR spectra arising from a system as in b) at two values of T_w. Numbers identify peaks discussed in the text.*

frequency with detection (probe) frequency (Fig. 1(c)). The laser pulses used are of ultrashort duration (~200 fs duration or less) while control of the time delays between them allows measurement of the evolution of the molecule's response with time, giving access to dynamic information. The most commonly-used of these delay times is the waiting time at which a 2D-IR measurement is recorded (T_w, Fig. 1(a)), which can be varied to measure effects arising from vibrational relaxation and solvent-solute dynamics. An additional benefit of the non-linear spectroscopic nature of the measurement is a slight narrowing of the measured linewidths of the bands on the spectrum diagonal,[1] providing improved frequency resolution compared to FT-IR.

From a practical perspective, a 2D-IR spectrum can be understood effectively as a frequency-resolved pump-probe experiment.[1] The method and general form of the spectra have been reviewed in detail many times and so this will not be repeated here[1, 4-9], but it is necessary to provide a brief overview to inform later discussion. To do this, we consider an example spectrum of a model molecule featuring two coupled vibrational modes, *a* and *b* (Fig. 1(b)). A schematic diagram of the relevant vibrational energy levels are shown in Fig. 1(b), which includes both the v = 1 (labelled as *a* or *b* in the figure) and the v = 2 (*2a*, *2b*) vibrational energy levels, which can be accessed as a result of the pump-probe nature of the experiment. Also shown is the combination band (*ab*) which features one quantum of excitation in both modes.

Considering the 2D-IR spectrum of this system obtained at a short value of T_w (250 fs, Fig. 1(c), left), it can be seen that the two fundamental vibrational transitions (v=0-1) for modes *a* and *b* appear on the

diagonal of the 2D-IR plot, labelled **1** and **2**. At room temperature, these are the only transitions that would appear in an FT-IR spectrum of this molecule as only the ground vibrational state is appreciably populated. In a 2D-IR experiment the pump pulse is used to excite the modes before a time-delayed probe detects the state of the system as a function of T_w. In Fig. 1(b) it can be seen that this leads to the appearance of peaks due to the v=1-2 transitions of *a* and *b* (peaks **3** and **4**), which are shifted to lower probe frequency relative to the diagonal peaks by the anharmonicity of the mode in question. As modes *a* and *b* are vibrationally coupled (excitation of one leads to a change in the frequency of the other) two further peaks appear in the off-diagonal region at the frequency of the coupled mode (labelled **1'** and **2'**), creating a square set of peaks (see dashed box) that can be used to identify any pair of coupled modes. Two final peaks (**5** and **6**) arising from transitions from the v=1 levels of *a* and *b* to the '*ab*' combination band are also visible. The separations of the off-diagonal pairs of peaks (**1'** & **6**; **2'** & **5**) report on the off-diagonal anharmonicity of the combination band relative to the energy of the two fundamental transitions, which provides a measure of the coupling strength of the two modes.

As T_w is allowed to increase (Fig. 1(c), right panel), the peaks in the 2D-IR spectrum reduce in intensity. This is caused by the relaxation of molecules from higher vibrational energy levels to the ground vibrational state. However, some new off-diagonal peaks also appear (see numbered peaks in the right hand spectrum of Fig. 1(c)) which were not present at shorter values of T_w. These are labelled according to the transitions that they correspond to in Fig. 1(b) and it can be seen that they occur because of energy transfer between the v=1 levels of modes *a* and *b.* The rise times for these peaks can be used to measure energy transfer pathways between modes.

The additional information content from a 2D-IR spectrum relative to FT-IR, even for a molecule with a relatively simple set of vibrational modes, is clear from Fig. 1. Overall, 2D-IR is able to identify coupled modes, which can be used to aid assignments or unravel spectra of mixtures. Different polarisation relationships between the pulses that generate the 2D-IR signal can be used to extract information regarding the angles between the transition dipole moments of the coupled modes, and so yield direct structural insight.[2] The changes in peak heights with T_w provide energy relaxation information, which is linked to solvent-solute interactions or intramolecular vibrational energy redistribution pathways.[10-12] The growth of off-diagonal peaks can also be used to reveal chemical exchange between two species in equilibrium.[4, 13, 14] Finally, though not shown in the example, for samples where the vibrational lineshapes are inhomogeneously broadened, for example molecules in H-bonding solvents, the 2D-IR lineshape and its evolution with T_w can be used to extract the underlying dynamics of the processes causing the broadening, such as the H-bond exchange timescale.[15-18] The range of timescales of the dynamics that 2D-IR is able to access are determined at the upper limit by the vibrational lifetime of the mode being studied (typically on the order of 1-150 ps) and at the lower limit by the time resolution of the instrument (typically 100-200 fs). This means that, although the range is relatively narrow, it encompasses a number of important molecular processes, from rotational motion to isomerisation, and H-bond exchange that are all difficult to measure with other methods. This gives 2D-IR a place in the general suite of tools that can be used to study molecular systems. In addition, the ability to measure a molecule-specific 2D fingerprint linked to structure makes 2D-IR potentially a powerful technique for analysis of complex samples.[3, 8, 19, 20]

The ability to provide detailed insight into the fundamental relationships between vibrational modes and their interaction with the molecular environment has led to a range of different applications for 2D-IR over the course of the 26 years since its first use.[21] These include probing solvation dynamics[12, 13, 22-30] and uncovering the ultrafast processes involved in catalytic mechanisms[31-35] as well as biochemical or biophysical applications, from assessing the role of environment in hydrogenase active sites,[29, 33, 36, 37] to examining the structural fluctuations of proteins and DNA.[38-51] Indeed, it is in relation to biomolecular samples that 2D-IR has perhaps made the biggest impact thus far. The intricately-coupled, delocalised modes, such as the amide I mode, that arise from the folding of peptide chains into protein secondary structures and from the intramolecular couplings of DNA bases in double-stranded DNA lead to 2D-IR spectral signatures that are very sensitive to 3D-structure, dynamics and interactions such as ligand binding. Recently, this has extended towards the possibility of applying 2D-IR to analytical problems,[3, 52, 53] made possible by the ability to study proteins in H_2O-rich fluids using 2D-IR.[19,54,19, 55] This has enabled 2D-IR studies proteins in physiologically-relevant solvents, where drug binding and protein structural changes have been explored.[56-58]

In the rest of this review, we focus on recent technological and data processing developments in order to show how they have contributed to a growing breadth of applications of 2D-IR spectroscopy. We then consider how this provides a platform for future directions and the feasibility of a transition for 2D-IR from specialist technique to accessible laboratory tool.

Recent Advancements

Instrumentation

Since 1998, the progression of 2D-IR applications has been closely linked to the development of the associated laser technology. At the outset, two methods existed for measuring 2D-IR spectra; a frequency domain approach where the pump frequency was scanned by placing a tuneable spectral filter in the pump beam, and a time domain method where the time delay between the two pump pulses (τ in Fig.1(a)) is scanned and a Fourier transform used to recover the pump-frequency axis of the spectrum in a manner akin to FT-IR spectrometers.[1, 6, 59] The frequency domain method provided a lower time resolution measurement than the time domain method and is now used relatively rarely. Similarly, more than one method of implementation exists for the time domain approach. The initial experimental design placed the three beams of input laser pulses at three corners of a square, the so-called boxCARS geometry. This led to the signal pulse being emitted by the sample towards the fourth corner of the square and so allowed a background-free measurement. This is perhaps the most sensitive 2D-IR collection method, but requires separate alignment of a local oscillator laser beam to achieve heterodyne detection. Careful phasing of the Fourier transformed data is also necessary to avoid distortions of the lineshapes that are caused by imperfections in the measurement of the time delay between the laser pulses.[1, 6] The second time domain method arranges the three input pulses into a pump-probe beam geometry, with two 'pump' pulses and one probe (Fig. 1(a)). This approach considerably simplifies data collection and analysis by using the residual probe beam as an intrinsic local oscillator. When the pulses are generated by a pulse shaper,[60] this experimental arrangement also removes ambiguity over the relative pulse timings allowing straightforward generation of 2D-spectra

without artefacts. At the current time, the choice of time domain implementation method is largely governed by considerations such as the need for overall sensitivity and control of the pulse sequence versus simplicity, robustness and speed of data collection, which are in turn dictated by the application. Significant improvements continue to be made in 2D-IR instrumentation, which we broadly categorise into three main areas: laser sources, detectors, and sample handling strategies, each of which has led to advances in the technique.[21] We review each of these areas separately below, focusing on the specific benefits, for example in terms of speed of acquisition, sensitivity or reproducibility of the instrument.

Laser Sources

Perhaps the most telling single step advance in 2D-IR capability of the last decade is the advent of high pulse repetition rate Yb-based laser systems. Historically, the majority of 2D-IR spectrometers have exploited regeneratively amplified Ti:sapphire laser systems, capable of producing pulse repetition rates from 1 to 10 kHz.[61, 62] These laser systems became commercially available in the 1990s[63] and provided the ability to successfully pump optical parametric amplifiers for IR pulse generation.[6]

In the past 5-10 years, high repetition rate Yb-laser technology has emerged as a natural successor to Ti:sapphire.[62, 64] By producing higher average powers and much greater pulse repetition rates (up to 100 kHz), Yb-based systems yield advantages ranging from faster data acquisition rates and greater experimental throughput to superior shot-to-shot stability and improved signal to noise ratio.[62] In addition, Yb-lasers confer advantages in efficiency, reduced footprint and cost effectiveness, consuming approximately an order of magnitude less electrical power than Ti:sapphire systems.[62, 65] As these lasers derive from commercial or industrial laser platforms they tend to be more robust and low-maintenance than a Ti:sapphire laser, focusing experimental effort and development on to the spectroscopy measurement rather than laser alignment, which enables more ambitious applications to be undertaken.

The first reported use of a 100 kHz Yb:YAG amplifier for 2D-IR applications was documented by Luther *et al.* in 2016.[65] The system was designed using a diode pumped Yb fibre oscillator and cryo-cooled Yb:YAG amplifiers, with a single oscillator generating both the seed and pump beams.[65] With this system, Luther *et al.*[65] were able to achieve high efficiency and high repetition rates to generate a 2D-IR spectrum of potassium cyanate, with a single spectrum collected in 7.6 ms.[65]

The same year, Greetham *et al.*[66] reported the use of a 100 kHz Yb:KGW laser for time-resolved spectroscopy, though not yet 2D-IR experiments. Comparing directly with a spectrometer using a Ti:sapphire laser showed that the latter demonstrated a noise intensity 5 to 10 times greater than the Yb-amplifier.[66] Given that laser stability directly correlates to the signal-to-noise ratio of the resulting spectrum, the implication was that higher repetition rate Yb-based amplified systems not only offer greater data acquisition speed but improved signal-to-noise ratios.

Slightly later in 2016, this same laser system was used for a series of 2D-IR spectroscopy experiments mapping the energy relaxation pathways of double-stranded DNA from base vibrational modes to those of phosphate backbone.[67] The instrument itself was described in detail in 2018,[68] where the authors demonstrated an improved signal-to-noise ratio with the Yb:KGW system offering a 3 to 10 fold

improvement over a 1 – 10 Hz system, at data collection rates between 10 to 100 times faster.[68] This improvement in signal-to-noise was matched by Farrell *et al.*[61] who noted an 8 fold improvement in comparison to their Ti:sapphire laser.[61]

It is important to acknowledge that although high repetition Yb-based systems offer improved data acquisition speed and sensitivity, this comes at the cost of reduced spectral bandwidth, generating pulses typically 2 to 3 times narrower than their Ti:sapphire counterparts, with concomitant reductions in temporal resolution due to the longer pulse lengths.[68] To understand the impact of the reduced spectral bandwidth and to assess the performance of the Yb:KGW amplifier system, Donaldson *et al.*[68] focused on samples exhibiting strong carbonyl stretching frequencies.[68] Of note was the system's ability to monitor spectral diffusion on the 250-300 fs time scale, in addition to improved detection sensitivity for weak signals, with detection down to nM levels.[68] Importantly, the study found that the reduced spectral bandwidth did not hinder the 2D-IR measurements, thus making the 100 kHz laser system suitable for integration into a 2D-IR spectrometer.[68] It is important to note however that, while no detriment was found for samples where focus was placed upon the carbonyl stretches in the amide I and II regions of interest, this may not be the same for alternative sample types with other vibrational frequencies. As such, careful consideration still needs to be given to spectral bandwidth when determining whether the spectrometer characteristics meet the needs of the experiment.

As the benefits of high repetition lasers become evident, their use for 2D-IR experiments is steadily growing.[52, 56, 57, 61, 65, 68-73] Other implementations have included their use in transient 2D-IR experiments where photoactivated systems can be followed with 2D-IR experiments on timescales from microseconds to milliseconds.[69] Future developments in laser technology are expected to address the challenge of spectral bandwidth in high repetition rate Yb-based laser systems. When coupled with advancements in laser manufacturing processes, including cost reduction and perhaps miniaturisation and new gain materials, it is expected that improvements in laser sources will drive continued advances in 2D-IR spectroscopy applications in the years to come.

Detectors

The advances in laser sources have prompted a need for complementary improvements in other aspects of spectrometer systems. Studies have highlighted that while 100 kHz Yb-based laser systems offer significant benefits, the major component of system noise often stems from the detector rather than the laser.[66] Donaldson *et al.* emphasised the importance of implementing shot-by-shot detection to fully leverage the increased signal-to-noise offered by the 100 kHz laser, once again underscoring the reliance on detector performance as a primary factor in overall performance. [62] Pulse detection has historically been achieved through various methods, including up-conversion of mid IR pulses to visible wavelengths[11, 74, 75], full time domain measurement methods using single pixel mercury cadmium telluride (MCT) detectors[76-78], or more commonly dispersing the signal using a spectrometer and detecting using multi-pixel MCT arrays (Fig. 1(a)).[4, 61, 68, 77, 79, 80] The latter are typically composed of between 32 and 128 pixels, facilitating a range of spectral resolutions, depending on the laser bandwidth and the specifications of the grating spectrometer used to disperse the signal onto the array.[61, 62, 66, 68] An alternative to traditional linear MCT detection systems was introduced by Ghosh *et al.*[79] who utilised

a MCT focal plane array (FPA) detector system. The FPA design, similar to charge-coupled device (CCD) camera systems, has demonstrated success in other spectroscopic techniques such as FT-IR microscopy.[79, 81] Commercially available FPA-MCT detectors offer a 128x128 pixel configuration and fast readout times, making them well-suited for applications in ultrafast spectroscopy and also microscopy applications.[82, 83]

Utilising NaN_3, Ghosh *et al.*[79] compared 2D-IR spectra from a 32-pixel linear MCT detector with those from an MCT FPA under identical collection conditions.[79] The direct comparisons of 2D-IR contour plots and slices through the spectrum revealed the FPA detector to be a viable alternative, exhibiting improved line shape and better sampling due to its increased number of detector pixels compared to the linear 32-pixel MCT array.[79] When assessing signal reproducibility across 400 scans, both detector systems demonstrated comparable relative standard deviations (RSD) of the absolute peak intensity, albeit the FPA exhibited a slight advantage with a ~ 4% decrease in RSD, measured at 29.5% for the linear MCT and 25.7% for the FPA.[79] A comparison of the pixel noise between the two systems yielded similar results. To further evaluate the performance of FPA detector systems, the authors assessed their suitability for investigating real-time dynamics, analysing a $W(CO)_6$ complex without employing averaging, thus utilising a single shot for each coherence time (τ in Fig. 1(a)) point.[79] The authors found that more significant improvements in detection sensitivity could be achieved by combining the FPA alongside a reference subtraction strategy. This lead to the extraction of clearer 2D-IR peaks above the background noise, achieving a signal to noise ratio 4 times greater than observed with the FPA alone, with detection in a matter of milliseconds.[79] Overall, Ghosh *et al.'s* FPA-based detector system demonstrated promise as a viable alternative to traditional linear based MCT systems, where FPA can offer improved performance, wider spectral bandwidths and easier simultaneous collection of a reference beam. [79] Despite this, the utilisation of MCT FPA arrays for 2D-IR purposes remains limited. To the best of our knowledge, only two subsequent studies have been published utilising the 128x128 pixel MCT FPA: one by Stingel *et al.*[84] in 2021 for the analysis of semi-conductor samples, and Week *et al.*[85] in 2022 for the monitoring of peptide self-assembly.[84, 85]

A further advance in technology related to the advent of high pulse repetition rate lasers focused not on the detector but on the electronics and signal processing. By designing a system specifically for shot-to-shot operation while minimising noise and optimising signal processing speed, the intention was to allow signal acquisition methods to keep up with the increases in laser repetition rate.[61]

Sample handling:

Another area where significant development has occurred in recent years is in improving sample handling and presentation techniques, expanding 2D-IR beyond the transparent solutions that have dominated its early development. While 2D-IR has been successful for the characterisation of systems with a limited number of components, the potential for broader applications lies in the analysis of more complex or solid-state samples or inhomogeneous biological samples such as cells.[86, 87] 2D-IR measurements are typically performed by sandwiching a liquid sample between two IR transmissive windows, such as Ca_2F, to maintain controlled pathlengths during measurement.[3] Traditionally, researchers aimed for optimum sample transparency to minimise the presence of particulates that

cause unspecific scattering of incident pump light.[70, 86] This generally manifests along the diagonal of a 2D-IR spectrum, obscuring the information-rich spectra.[70] While strategies such as phase cycling, polarisation control or multi-variate analysis can mitigate this in mostly transparent samples, these processes become less effective in cases of extreme scattering such as with opaque or solid samples.[70, 88-92] In such scenarios, where scattering effects dominate the spectra, alternative sampling protocols are required. This underscores the importance of advancing sample handling techniques to address the challenges posed by scattering in 2D-IR spectroscopy, paving the way for broader applications in the analysis of complex and solid-state samples.

One such protocol involved the utilisation of a dispersal technique with refractive index matching oil. Index matching entails dispersing the solid sample within an oil that shares the same refractive index as the IR transmission windows. This minimises distortion and reflection at the sample interface, facilitating the removal of sample scatter.[70, 93] While index matching can effectively reduce scatter for linear spectroscopy techniques, it may not suffice for multidimensional applications. Yan *et al.*[93] demonstrated that index matching with Nujol oil still left a significant contribution from scatter obscuring the spectra. Consequently, it became necessary to combine index matching with scatter subtraction strategies utilised for transparent samples. The authors opted to use a scatter subtraction strategy previously employed by Nishida *et al.*[94] for analysing crystalline metal-organic-frameworks (MOFS). [94] This strategy proved successful in scatter suppression, enabling clear identification of the 2D-IR peaks, as demonstrated within Figure 2.[94] This scatter reduction strategy utilises a perpendicular pump-probe 2D-IR <XXYY> set up, where pulses 1 and 2 (YY) have a perpendicular polarization relative to pulse 3 and the echo (signal) pulse (XX). The combined pulse 3/signal pulse is then passed through an X resolving polarizer, filtering out a substantial amount of the scatter from pulses 1 and 2. Any remaining scatter was further reduced by an 8-shot phase cycling scheme.[93, 94]
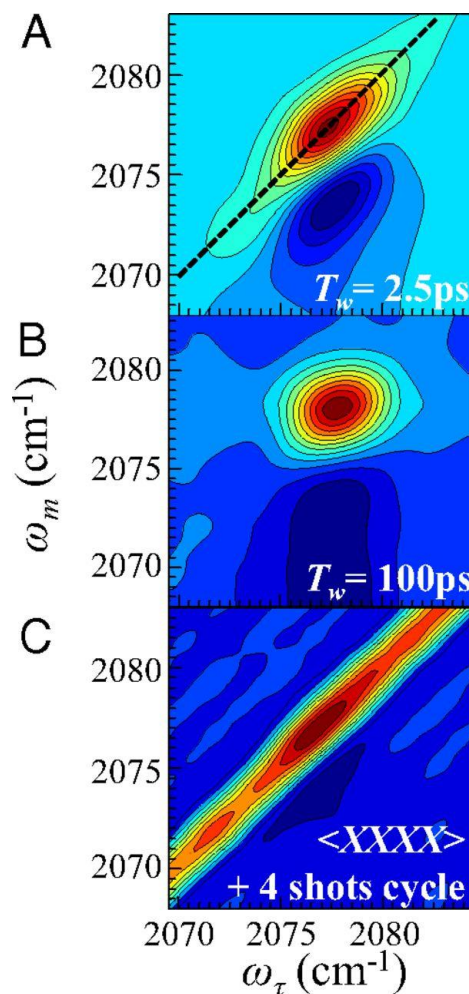
Figure 2: *2D-IR spectra demonstrating the scatter suppression when utilising the <XXYY> polarisation, 8-shot phase cycling strategy for the measurement of Ui-O66 MOF by Nishida et al.[94]. Where (A and B) demonstrate the resultant spectra with scatter suppression and (C) without. In this data, ω_m and ω_τ correspond to the probe and pump frequency axes as shown in Fig. 1(c). Reproduced with permission from Nishida et al.[94] Copyright (2016).*

Using this approach, Yan *et al.*[93] successfully monitored the hydration dynamics of minerals gypsum and bassanite using 2D-IR spectroscopy.[93] The resulting spectra were free of scatter, exhibiting clear line shapes that facilitated accurate interpretation of the dynamic water processes occurring within the granular powders. This method has been used elsewhere, effectively removing scattered light and resulting in spectra with clear line shapes suitable for elucidating dynamic processes.[95, 96]

While index referencing combined with chopping, phase cycling and polarisation steps was shown to be an effective method for analysing samples with significant scatter, this approach may not always be suitable depending upon the sample, and it can increase preparation time which reduces sample throughput. An alternative method for solid-state samples has been investigated that does not require the use of index matching oil. In 2023, Donaldson *et al.* reported spectra of highly scattering pelleted zeolites.[70] By combing a bright probe beam with a 4-shot phase-cycling technique, they exploited the relationship of probe light intensity with heterodyne and direct scatter. This revealed that an n factor

increase in probe intensity results in a decrease in heterodyne and direct scatter by a factor of $\sqrt{n}$ and n respectively, while the 2D-IR signal intensity remains independent of probe intensity.[70] By increasing the probe incident light from ~ 10 to 20 nJ/pulse to 0.5 to 1 μJ/pulse, the authors observed a significant decrease in scatter. The incorporation of <XXYY> polarisation further reduced scatter, enabling the identification of more defined spectral features, as illustrated in Figure 3.[70]
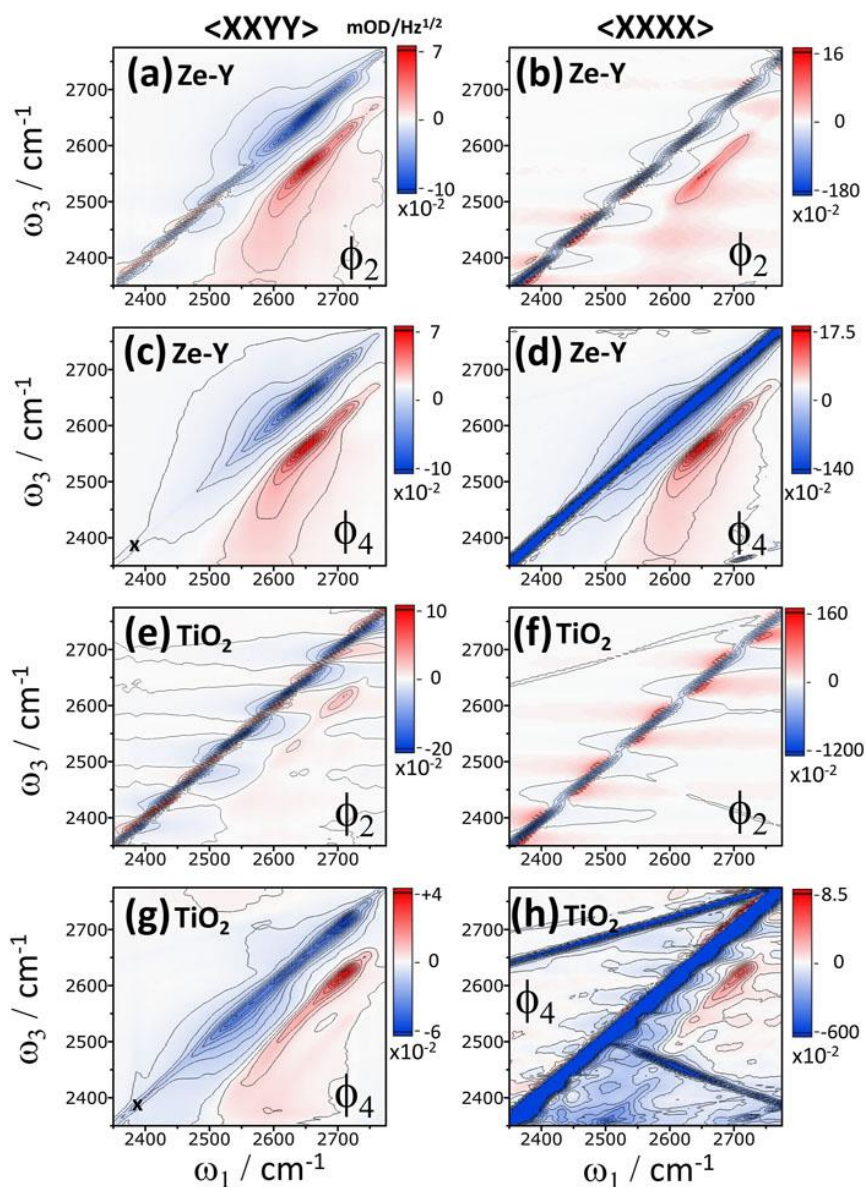

Figure 3: *2D-IR spectra obtained for zeolite Y and TiO$_2$ by Donaldson et al. utilising probe light intensity, phase cycling and polarization scatter reduction strategies. Perpendicular polarization <XXYY> strategies are shown in the left-hand column and parallel <XXXX> in the right, with four-frame scatter suppressing phase cycling denoted by "ϕ_4" and two-frame non-scatter suppressing phase cycling denoted by "ϕ_2". Reproduced with permission from reference[70].*

While the use of increased probe intensity in combination with perpendicular polarisation offers an alternative scatter suppression strategy without the need for refractive index matching, some on-

diagonal scatter remains apparent in the resultant 2D-IR spectra, which cannot be fully removed by this protocol.[70] Therefore, while it represents a step forward in collecting spectra of highly scattering solid samples, a comparison of the outlined scatter reduction strategies (Figure 2 and 3) suggests that the inclusion of refractive index matching remains the primary strategy alongside polarisation and phase cycling for obtaining high-quality spectra of solid samples. These techniques offer better opportunities to accurately study dynamics within solid-phase samples.

Another recent development in sample handling is the integration of microfluidics, aimed at increasing sample throughput for solution phase samples in an effort to match sample delivery with enhanced laser performance. Microfluidic systems offer several advantages over traditional static cell sampling strategies, including improved control over sample flow, reduced sample volume requirements, and enhanced mixing capabilities. These advances have the potential to significantly enhance the efficiency and capabilities of 2D-IR spectroscopy experiments. Tracy et al.[97] demonstrated such an approach in 2016 by integrating microfluidic systems with 2D-IR spectroscopy for the interrogation of solvation dynamics, specifically focusing on the pseudohalide cyanate anion.[97] The authors combined a microfluidic cell with a 100 kHz high-repetition rate laser to maximize efficiency, although noted that the cell could easily be incorporated with any laser system.[97] Although scatter was observed in 50% of the measured spectra, likely due to measurement position lying close to the edges of the microfluidic channels, they did find that when measurement position was optimised within the channel spectra collected were comparable to those obtained from static CaF_2 measurements.[97] Of note however, was the remarkable ability of the combination of the microfluidic cell with the high-repetition laser facilitating the collection of 1600 fully averaged spectra in 125 minutes, achieving a higher throughput 2D-IR system, averaging 12 spectra per minute.[97] Despite the initial promise demonstrated by Tracy et al.[97], there have been relatively few documented combinations of microfluidic cells with 2D-IR since, although the technology has been more widely employed in FT-IR applications. A recent study by Giubertoni *et al.*[98] in 2023 showcased the combination of microfluidic devices with 2D-IR spectroscopy for multidimensional IR diffusion-ordered spectroscopy (DOSY).[98] Utilising a 1 kHz Ti:sapphire laser system, the authors successfully distinguished protein amyloids and monomers within a mixed sample.[98] This approach offers an alternative benefit to the increased throughput demonstrated by Tracy *et al.*[97], demonstrating the versatility of microfluidic integration with 2D-IR spectroscopy. The integration of microfluidic technology with 2D-IR spectroscopy holds promise for further improvements in sample efficiency and data acquisition. As the combination of these techniques continues to evolve, it is expected to contribute to enhanced analytical capabilities and expanded applications in various fields.

Data analysis

The preceding examples have shown the remarkable progression of the 2D-IR method over the last 26 years. It is clear that as 2D-IR continues to develop over the next 26 years, the speed at which high-quality, large data sets can be acquired is going to become either a significant problem or opportunity for the field. The problem arises from the fact that while traditional spectrum by spectrum analysis will still be valid for simple datasets, perhaps through measuring the spectrum of a single or small number

of samples over a range of waiting times, exploiting fast data acquisition will require more sophisticated approaches. This leads to the opportunity of interfacing 2D-IR with data analysis methods such as Machine Learning (ML) that have already become prominent in other, more data-rich, fields. ML models are increasingly being applied in spectroscopy,[99] either for diagnostic purposes, e.g. to examine structural-spectral relationships by predicting spectra from structure and vice versa using large data libraries [100-102] or in a more applied setting such as discriminating cancerous from non-cancerous cases in big sets of data obtained from patient samples.[103-106]

To capitalize on this opportunity, ML and other intelligent processing and analytical tools must be developed alongside 2D-IR to both handle the 'big data' and unravel the complex spectra. There are already signs of this, particularly focused around research to transfer 2D-IR to clinical or pharmaceutical applications for biomedical diagnostics and drug design applications[3, 20, 54, 56, 57, 71, 107]. The challenge can be considered in two parts; (1) the automation of spectral pre-processing steps that account for measurement-to-measurement and instrument-to-instrument variability, and (2) the development of machine learning tools that can efficiently handle, and accurately analyse, the large and complex datasets. Significant steps towards proof of concept for the value of pre-processing tools have been made by Rutherford *et al.*[52] who, inspired by workflows established for other spectroscopic disciplines, constructed a workflow for 2D-IR spectra, based on samples of proteins in H_2O-rich fluids.[52] Importantly, the final step introduced a label-free internal normalization standard for the protein amide I signal – a water thermal response that appears at later delay times (~ 5 ps). It was found that both signals are impacted similarly by sample- and instrument-related variations, meaning that there exists a linear correlation between their absorbances, irrespective of sample concentration. This enabled exact concentrations to be extracted from the 2D-IR spectra, necessary for quantitative analytical applications, improved data interpretability, and accounted for the path length variability that is introduced when measuring protein samples in H_2O.[55] The other steps in the workflow included the standard zero padding, apodization and Fourier Transformation of raw 2D-IR data,[1] alongside baseline correction, Savitzky-Golay smoothing, and principal component analysis (PCA)-based noise reduction. Upon application of this workflow to previously collected datasets,[55, 107] the authors found significant improvements in signal to noise ratio, and in the case of quantifying glycine concentrations in spiked equine serum, the detection limit reduced from 3 to 0.8 gL^{-1}. It was explained that this would serve as an upper sensitivity limit since coupling in more complex protein secondary structures would increase the signal intensity of the amide I band. This highlights how such pre-processing steps would be imperative for analysis of samples either with low signal intensities, or real physiological samples where natural protein concentrations can be very low.[108, 109] In combination with surface enhanced IR spectroscopies employing photonic near-field enhancement that improve light-matter interactions,[110] this could further reduce the detection limit for IR spectroscopies.

Even with such pre-processing tools, the next step of deriving spectral insight from large quantities of information is a difficult task. ML-based tools in which a machine, or computer, recognises and learns associations or patterns within a dataset could potentially assist with this.[99, 111] The potential for ML methods has been demonstrated to the fields ranging from speech and image recognition,[112-115] defect

and crack detection in materials[116] to screening of drug candidate molecules[117] and the enhancement of quantum mechanical calculations.[118]

ML models are constructed through training and subsequent testing using different sets of data, and can be generally categorized by their style of learning, i.e. supervised or unsupervised, and the task they are designed to perform, i.e. regression or classification (or both). In supervised learning, the data is labelled (e.g. a cancerous or non-cancerous sample) whilst in unsupervised learning, the data is not labelled. Often supervised learning can aid classification and, as such, increase the accuracy of a model, but can introduce subjectivity and bias.[72, 99] Unsupervised learning, however, is objective and can be useful when variables of the dataset are unknown, e.g. spectral features that arise from certain characteristics of the sample. It has also been argued that unsupervised learning functions much more like the human brain than supervised learning since we *'discover the structure of the world by observing it, not by being told the name of every object'.[111]* It does, however, have the disadvantage of being more sensitive to outliers.[99] Ultimately, these different types of learning can be applied separately or in combination to perform a desired task. Classification ML models organise the data into two (binary) or more (multiclass) classes, with or without labels, based on certain patterns it recognises. Without labels, it is necessary for the user to have pre-existing knowledge about the dataset to aid interpretation of the resulting classification. Regression ML models predict continuous values, much like using a line of best fit to predict values based on the examples used to produce the line.[119-122]

When applied to spectroscopy, ML has the capability of transforming not just our understanding of a given system, such as in structural-spectral relationships, and handling large datasets for classification, but also in making the spectroscopies more accessible to non-expert users. Recently, ML models have been increasingly used in combination with linear vibrational spectroscopies (IR and Raman) for clinical diagnostics. Different studies have used dried human serum,[104-106, 123-125] plasma,[106, 124, 126] saliva and sputum,[127-129] tears,[130] and bladder wash[131] to identify cancerous[103, 104, 106, 124-126, 128, 129, 131-133] and diabetic[127] samples by employing multivariate analysis (MVA) techniques, such as principal component analysis (PCA),[106, 123, 124, 126, 129-131, 133, 134] and principal component regression (PCR),[125] hierarchical cluster analysis (HCA),[129] linear discriminant analysis (LDA),[124] k-nearest neighbours (kNN),[103, 106, 135] and other supervised machine learning techniques including support vector machines,[103, 105, 106, 135] and neural networks (NNs).[103, 104, 135] Often the fingerprint region of the IR spectrum (900-1800 cm^{-1}) is the focus of the analyses as it contains peaks related to proteins, lipids, nucleic acids and carbohydrates – all key biomarkers for different diseases and cancers.[105, 136-139] In some cases, specificities and sensitivities (a model's ability to predict true negatives and true positives, respectively) greater than 95% were achieved,[103, 105, 124, 126] with multiple instances of very high accuracies (~ 100%).[103, 106, 124, 126, 127] One study constructed a NN to discriminate between healthy and cancerous colon cells that gave 98.7% accuracy, 100% sensitivity and 97.1% specificity.[103] As these MVA techniques and their applications to diagnostics using linear vibrational spectroscopies have already been well reviewed, they will not be discussed in any more detail here and the reader is instead directed to the following.[72, 99]

2D-IR spectra contain more complex and well resolved information than linear IR spectroscopies that allow the investigation of previously inaccessible information, but make the analysis and interpretation

much more challenging. Implementing ML tools could bridge this gap – models will be trained on spectra that inherently contain more details of the system being analysed, leading to greater accuracies and more intelligent ML tools, that are, in turn, capable of unravelling the complex information.

Some MVA techniques have recently been applied to interpret 2D-IR spectra – monitoring either protein-drug binding[56, 57] or protein structural changes.[58, 140] The first drug binding study employed PCA to monitor the presence of paracetamol in spiked human serum at physiologically relevant concentrations.[57] PCA was able to reveal that increasing paracetamol concentrations were consistent with a reduction in the α-helix albumin signal, providing insights into the binding process. The authors were also able to measure paracetamol concentrations as low as 1 µg mL^{-1}. The second study used partial least squares discriminant analysis (PLS-DA) to monitor binding of paracetamol, cefazolin, warfarin and ibuprofen to proteins in human serum, achieving 92% correct separation of normal serum to that with drug binding and 75% correct separation on a per drug basis.[56] It was also argued for both studies that the amide I band essentially enhances the drug signal that would otherwise be too weak to detect. These results establish the prospect of 2D-IR in combination with ML being translated into biomedical fields, which could later expand on the linear IR investigations described above. 2D-IR also overcomes the issue of the overlapping H-O-H bending mode of H_2O with the amide I band.[55] Whilst the linear IR diagnostic studies outlined above utilize sample drying to bypass this issue, potentially introducing additional error into the experiments, 2D-IR would allow more physiologically relevant studies to be conducted.

Some other studies employing PCA investigated temperature-induced structural changes of calmodulin[140] and the antimicrobial peptide gramicidin A.[58] In both cases, PCA aided understanding of the structural origin of specific spectral features, giving quantitative insight into secondary structural changes[140] and the melting of protein aggregates.[58]

An insight into the types of outcomes that harnessing ML methods to larger datasets can generate can be seen from examples featuring either forward (predicting spectra from structure) or reverse (predicting structure from spectra) mapping. Forward mapping has been explored for K-edge X-ray absorption (XAS),[141] far-UV,[142] circular dichroism (CD),[143] and amide I and II linear IR absorption,[100, 144] spectroscopies using data generated by molecular dynamics (MD) or density functional theory (DFT) calculations, or extracted from the transition metal Quantum Machine dataset.[145] All studies constructed NNs with considerable accuracy, and some expanded their research to incorporate dynamical changes in structure, predicting the spectra of proteins with changes in temperature,[100] pH,[144] and across a folding path,[100, 142-144] again with great success. Despite this, some reported slight deviations between the ML predicted FWHM and position of bands in comparison to experimental data, which was assigned to the limitations of the computational methods (from which the data used to train the model was derived) in correctly capturing structural fluctuations under real conditions.[100, 144] This emphasises the need to include real experimental data when training ML models, rather than relying purely on computationally derived data.[146]

Reverse mapping for vibrational spectroscopies has been investigated using NNs trained on 21000 different computationally derived structures to recognise OH and CO bonds in molecules from IR and Raman spectra.[101] The authors reported a remarkable 99.36% accuracy for recognising OH bonds and

a 98.50% accuracy for recognising CO bonds. Ren *et al.*[102] used convoluted NNs trained on simulated linear IR absorption, CD and two-dimensional UV (2D-UV) spectra to predict the secondary structure of peptide fragments.[102] Models fed with 2D-UV data were found to be much more accurate (near 100%) than those fed with linear IR absorption (86-91%) or CD (87-93%) data, assigned to the presence of off-diagonal features that are only accessible to 2D spectra (Figure 4).
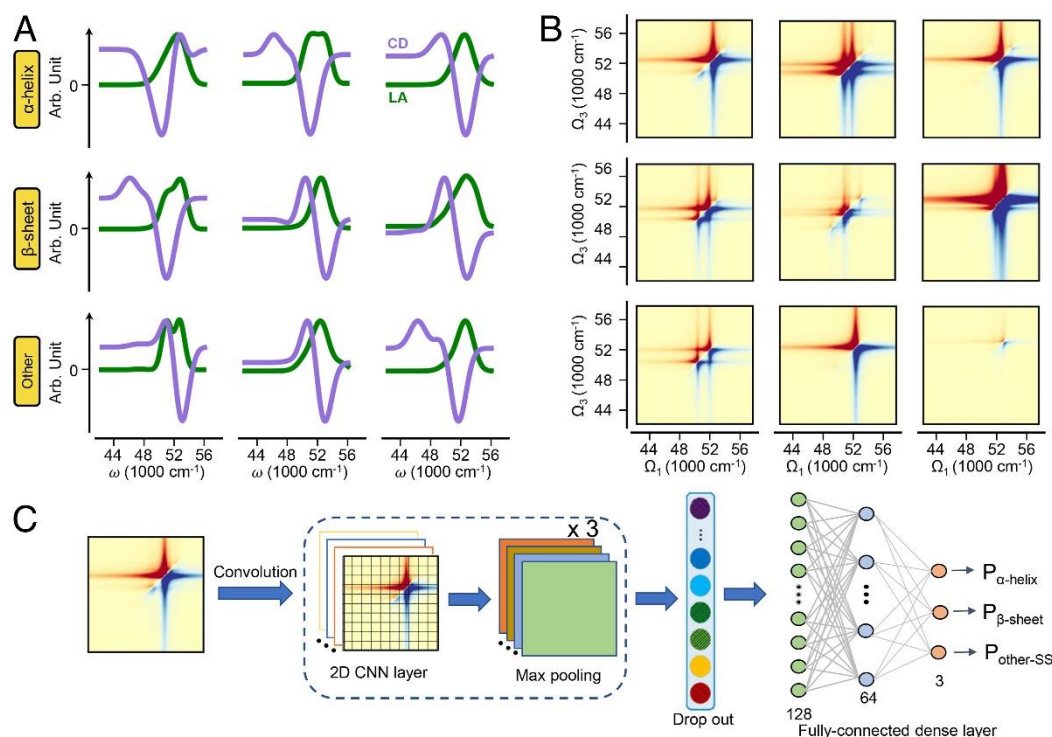

Figure 4: *(A) Linear absorption (green) and circular dichroism (purple) spectra of α-helical, β-sheet and other (unstructured) randomly selected peptide fragments, (B) the corresponding 2DUV spectra, and (C) the convoluted neural network architecture for secondary structure prediction from 2DUV spectra. Reproduced with permission from Ren et al.[102] Copyright (2022).*

This additional layer of structurally relevant information accessible only to two dimensional spectra clearly creates more intelligent tools. Therefore, considering the potential benefits of using ML in combination with 2D-IR, it is possible that these types of ML models could be trained with 2D-IR spectra. Alongside the femtosecond time resolution of the technique, this would place 2D-IR in a unique position amongst other commonly used structural analysis techniques. This niche has been investigated by Baiz *et al.*[49] who successfully demonstrated the use of singular value decomposition (SVD) to predict the fractions of secondary structural components of 16 different proteins in D_2O from experimentally collected 2D-IR spectra.[49] The set of proteins were especially selected to cover a broad range of α-helix and β-sheet compositions. Root mean squared errors comparing the SVD predicted values to those calculated from x-ray structures of 12.5% for α-helix, 9.2% for β-sheet and 9.1% for unstructured motifs were reported, values comparable to those derived from CD, the current standard for protein structural analysis. There now exists a significant opportunity to extend this proof of concept study towards larger

data libraries and physiologically relevant conditions.[55] Related to this, we note that AlphaFold has found great success in predicting static three-dimensional structures from crystallographic data.[147, 148] It is possible that the time resolved dynamical information contained within 2D-IR spectra, alongside the additional structural details captured by off-diagonal features, could allow ML models to learn and predict global and local protein dynamics, which is necessary to understanding their biological function.

Novel Applications

In this section, we summarise key advances in 2D-IR applications that have been enabled by changes in light source, detector or sample handling technology above, allowing an overview of the direction of travel of the field.

Since its inception, 2D-IR spectroscopy research has been dominated by applications to solution phase samples and biomolecules in general, with a particular focus on the amide I band of proteins.[21] More recently this has progressed to encapsulate work aiming to deliver analysis of biological fluids. Despite the ability of 2D-IR to circumvent the spectral congestion that arises when biomolecules are studied with linear IR techniques, 2D-IR faced challenges due to interference from H_2O.[19, 55] Initially, this obstruction was addressed by substituting D_2O for H_2O, effectively removing the interference at the 1650 cm^{-1} band of interest. For many years this method was adopted with great success and facilitated deeper understanding of dynamic and structural properties.[149-153] While this method provided a viable solution, there are concerns regarding the measurement of dynamics in an unnatural solvent, alongside the fact that practicality and increased costs limit widespread engagement with 2D-IR measurements. As previously discussed, the water suppression method developed by Hume *et al.*[55] began to enable the successful monitoring of proteins in aqueous and physiologically relevant environments.[19, 55] Since then, this method has been applied successfully for various fundamental and diagnostic studies.[52, 55-57, 71, 107] Several recent reviews have discussed in depth the application of 2D-IR spectroscopy for biomolecular analysis, with a particularly large focus on protein analysis.[3, 19, 154] While biomolecular and protein analysis remains a significant application area for 2D-IR spectroscopy, with a substantial amount of overall applications, we focus here on growing interest in developing application areas that will expand the scope of applications of 2D-IR, in an effort to demonstrate its potential future breadth.

In a notable study conducted by Ryan *et al.* in 2023, 2D-IR was employed for electrode surface analysis, focusing on the examination of hydrogen-bonding dynamics upon a nitrile-functionalised electrode surface.[155] This research is particularly significant considering the increasing adoption of electrochemical catalysis for compound synthesis, where understanding solvation dynamics at the electrode-solution interface could provide crucial advances.[155, 156] When an external voltage is applied to an electrode surface, the establishment of the electrical double layer and subsequent solution reorientation occurs, where electrostatic interactions repel or attract any charged species within the solution, influencing the surrounding chemistry.[155] Ryan *et al.* employed their custom-designed 2D-IR electrochemical cell[156] (Figure 5) to perform surface enhanced 2D-IR and investigate solvation dynamics at the surface of a self-assembled monolayer of nitrile-capped 4-mercaptobenzonitrile (4-MBN) functionalised gold electrode.[155] Ca$_2$F windows coated with thin layers of ITO and Al$_2$O$_3$ were used, followed by a plasmonic gold layer that enhances the spectroscopic signal.[156]

The authors observed significant changes in the 2D-IR spectral line shape over different timescales, indicating alterations in hydrogen bonding environments (Figure 5).[155] Notably, positive potentials were found to slow down the hydrogen bond breaking/forming between the nitrile and water molecules.[155] However, it is important to note that this study was conducted in deionized water, not under electrolyte conditions encountered in electrochemical cell reactions, suggesting further research is needed to fully understand solution-interface dynamics at electrode surfaces. Overall, the authors were able to demonstrate an interesting use of 2D-IR to enhance the understanding of the interface between the electrode surface and solution through the investigation of solvation dynamics under applied potentials.[155] This highlights how the potential for further collaboration between the two techniques of electrochemistry and 2D-IR spectroscopy could lead to fruitful advancements in both areas.

Beyond its application in interfacial studies at electrode surfaces, 2D-IR spectroscopy demonstrates additional synergy with electrochemistry. Recent examples include work using 2D-IR methods in combination with spectroelectrochemical cells to examine redox-related processes. This combination of techniques allows for the analysis of molecular dynamics in electrode materials, electrolytes, and reaction intermediates generated during electrochemical processes.[155-159] Dereka *et al.* recently utilised the technique to gain insights into the mechanisms behind a variety of battery electrolytes, distinguishing between chemical exchange and energy transfer, and to elucidate their scales.[159] The authors found that the chemical exchange occurs beyond the ultrafast timescale, typically within hundreds of picosecond, regardless of the exchange ion investigated.[159] Further discussion on the utilisation of spectroscopic techniques including 2D-IR can also be found in the recent review by Wang and Chen.[160] This research highlights the potential of 2D-IR spectroscopy to be involved in the advancement of energy storage and conversion technologies, such as batteries, fuel cells, and solar cells. By analysing the molecular dynamics of electrode materials, electrolytes, and reaction intermediates, researchers could further optimise performance to improve energy efficiency, and develop sustainable energy solutions for renewable energy applications.
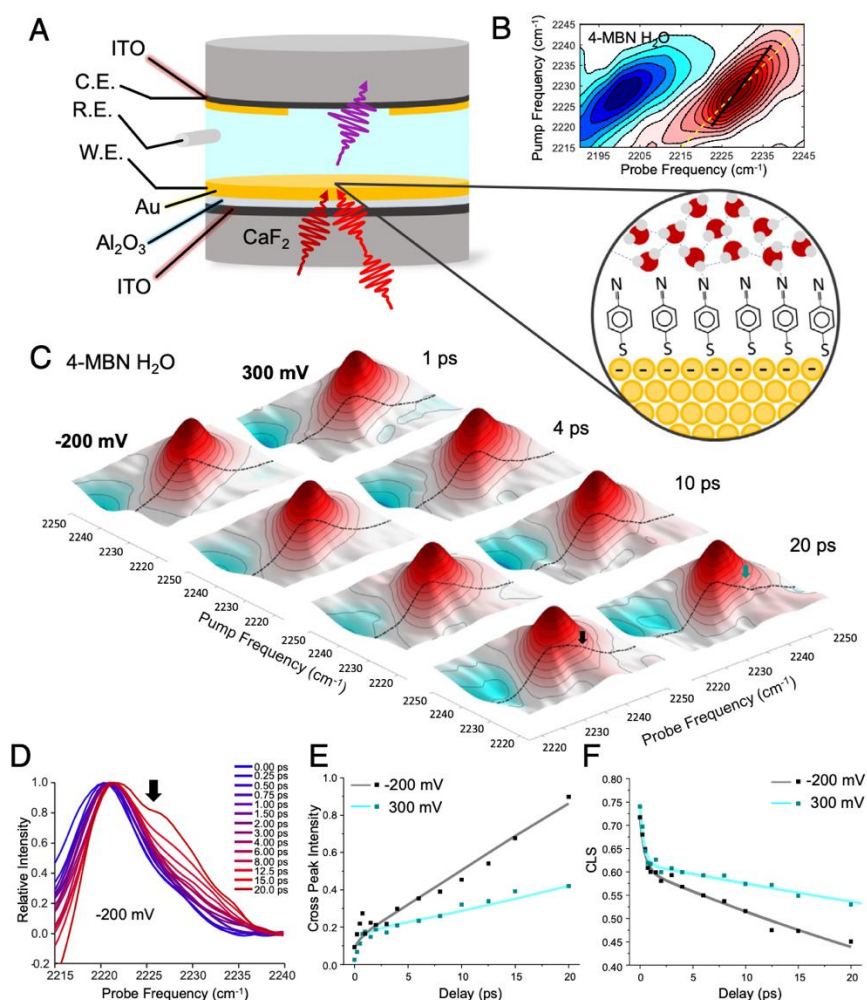
Figure 5: *Surface enhanced 2D IR spectra of 4-MBN upon the 2D-IR electrochemical cell designed by Yang et al.[156]. (A) Shows the construction of the 2D-IR cell, where the CaF_2 windows are coated wih a thin layer of ITO, followed by a buffer layer of Al_2O_3 and gold, where C.E., R.E. and W.E. stand for counter, reference and working electrode respectively. (B) Shows the resulting 2D-IR spectrum obtained for the analysis of the 4-MBN within water. The black line highlights the centre like of the ground state bleach. (C) Demonstrates the variation in line shape across different Tw and applied potentials. The black dotted line marks the 2220 cm^{-1} pump slice. (D) Shows the pump slices extracted from the 2D-IR spectra at -200 mV across the different Tw. The arrow highlights where the cross peaks appear. (E) Plots the cross-peak intensity response with Tw at 2227 cm^{-1} and finally (F) Shows the centre line slope of the 2D-IR spectra within plot (C). Reproduced with permission from ref [155] Copyright (2023).*

2D-IR spectroscopy is also emerging as a powerful tool for the characterisation of structure, composition and behavioural properties for a variety of materials, including polymers, composites, minerals and semi-conductors.[84, 93, 94, 161, 162] By providing the opportunity to unravel the intricate molecular architecture and dynamics of a variety of materials, material properties can be tailored with greater control, therefore accelerating the development of advanced materials likely to contribute to a variety

of applications from energy storage to biomedical devices. Additionally, the ability to probe molecular adsorption and interfacial dynamics, as demonstrated by Ryan *et al.*[155] and Yang *et al.*[156], has significant implications for catalysis, nanotechnology, and surface modification strategies. This interdisciplinary approach provides key insights not currently available with traditional characterisation technologies and opens up new avenues for innovation across multiple fields.[70, 163-166]

The application of 2D-IR spectroscopy now spans across numerous fields, driven by advancements in instrumentation and data analysis. From its traditional role in biomolecular studies to emerging areas of surface science, materials research, and analytical applications, 2D-IR spectroscopy offers improved precision and sensitivity in probing molecular structures, dynamics, and interactions. With opportunities to contribute to solving problems in disease diagnosis, energy storage and conversion, surface phenomena, and materials science, 2D-IR spectroscopy is in a unique position to help to address key challenges and drive innovation in diverse scientific and technological domains.

The Future of 2D-IR Spectroscopy: Looking Ahead to 2050

As we look toward the future of 2D-IR spectroscopy, the field appears poised for continued growth. The recent advancements in instrumentation, data analysis techniques and expanded applications provide a basis for believing that the method will continue to broaden its horizons, somewhat similarly to the ubiquity of applications now enjoyed by FT-IR methods.

While technology continues to improve, user-friendliness and ease of data analysis has not yet been achieved to the level where non-expert use of the technology is reasonable. As such, progress, perhaps leading to miniaturisation and cost reductions of laser sources, coupled with improvements in detector sensitivity and robust 'push button' spectroscopy equipment will be needed to change this. Despite the remarkable progress made in recent years, 2D-IR spectroscopy still faces several obstacles that must be addressed to realise its full potential. Chief among these is the need to overcome current limitations in sensitivity and signal-to-noise ratio. While advancements in laser technology have improved detection sensitivity and data acquisition speed, achieving sufficient sensitivity to detect trace analytes and low-concentration samples remains a challenge. Similarly, enhancing spectral resolution to resolve closely spaced vibrational modes and improving signal-to-noise ratios for weak signals are ongoing areas of research and development. The increasing complexity of 2D-IR spectra also demands advanced data analysis techniques to extract more meaningful information. Machine learning algorithms, in particular, hold great promise for enhancing spectral analysis, pattern recognition, and interpretation of spectroscopic data. By leveraging big data analytics and artificial intelligence, researchers may uncover hidden correlations, identify spectral signatures, and accelerate the discovery of molecular interactions and dynamics, thereby unlocking new insights into complex systems. It is plausible that these advances may yet underpin a transition to 2D-IR becoming more accessible.

The broadening scope of applications for 2D-IR spectroscopy is perhaps the most exciting aspect of its future. From its stronghold in solutions and biomolecular analysis to wider areas such as surface science, materials research, and analytical applications, these cases all reflect its increasing relevance and versatility across diverse scientific disciplines. In the study of surface phenomena, for example, 2D-

IR has allowed the probing of molecular vibrations at the interface between materials and their surroundings. In materials science, 2D-IR is emerging as a powerful tool for characterizing the structure, composition, and properties of materials, ranging from polymers to minerals, nanomaterials, and semiconductors. By fingerprinting molecular signatures and spectral patterns, 2D-IR stands to offer analytical insights into the identification and quantification of unknown compounds. In biomolecular analysis, 2D-IR has the opportunity to advance the probing of disease mechanisms, drug-target interactions, and therapeutic pathways. These expanded applications of 2D-IR demonstrate the potential of the technique to address complex scientific and technological challenges across various fields.

By 2050, we anticipate 2D-IR spectroscopy to have become more widespread tool in scientific research, industrial applications, and clinical diagnostics. Parallels might be drawn with NMR spectroscopy which took over 75 years to progress from first implementation to commercial instrument. With advancements in instrumentation enabling high-throughput, real-time measurements, and bench-top devices, 2D-IR spectroscopy could yet contribute strongly to fields such as pharmaceuticals, healthcare, and material science. As our understanding of complex systems continues to deepen, fuelled by advances in data analysis and machine learning, 2D-IR spectroscopy will play a role in advancing understanding as an addition to our armoury of analytical tools.

In conclusion, after 26 years of development, 2D-IR spectroscopy still offers promise. Continued innovation and collaboration within the scientific community will hopefully demonstrate the types of applications and potential markets which allow 2D-IR spectroscopy to take the next steps toward mainstream technology.

References

1. P. Hamm and M. Zanni, *Concepts and methods of 2D infrared spectroscopy*, Cambridge University Press, 2011.
2. M. Khalil, N. Demirdöven and A. Tokmakoff, *J. Phys. Chem. A*, 2003, **107**, 5258-5279.
3. R. Fritzsch, S. Hume, L. Minnes, M. J. Baker, G. A. Burley and N. T. Hunt, *Analyst*, 2020, **145**, 2014-2024.
4. S. Park, K. Kwak and M. D. Fayer, *Laser Physics Letters*, 2007, **4**, 704-718.
5. S.-H. Shim and M. T. Zanni, *Phys. Chem. Chem. Phys.*, 2009, **11**, 748-761.
6. C. T. Kuhs, B. M. Luther and A. T. Krummel, *IEEE Journal of Selected Topics in Quantum Electronics*, 2019, **25**, 1-13.
7. C. R. Baiz, M. Reppert and A. Tokmakoff, *Ultrafast Infrared Vibrational Spectroscopy*, 2013, 361-404.
8. N. T. Hunt, *Chem. Soc. Rev.*, 2009, **38**, 1837-1848.
9. M. Khalil, N. Demirdöven and A. Tokmakoff, *J. Phys. Chem. A*, 2003, **107**, 5258-5279.
10. A. I. Stewart, I. P. Clark, M. Towrie, S. K. Ibrahim, A. W. Parker, C. J. Pickett and N. T. Hunt, *J. Phys. Chem. B*, 2008, **112**, 10023-10032.

11. K. J. Kubarych, M. Joffre, A. Moore, N. Belabas and D. M. Jonas, *Opt. Lett.*, 2005, **30**, 1228-1230.
12. V. F. Crum, L. M. Kiefer and K. J. Kubarych, *The Journal of Chemical Physics*, 2021, **155**, 134502.
13. M. D. Fayer, D. E. Moilanen, D. Wong, D. E. Rosenfeld, E. E. Fenn and S. Park, *Accounts of Chemical Research*, 2009, **42**, 1210-1219.
14. D. E. Rosenfeld, K. Kwak, Z. Gengeliczki and M. Fayer, *J. Phys. Chem. B*, 2010, **114**, 2383-2389.
15. M. C. Thielges, J. Y. Axup, D. Wong, H. S. Lee, J. K. Chung, P. G. Schultz and M. D. Fayer, *J. Phys. Chem. B*, 2011, **115**, 11294-11304.
16. D. E. Moilanen, D. Wong, D. E. Rosenfeld, E. E. Fenn and M. D. Fayer, *Proc. Natl. Acad. Sci.*, 2009, **106**, 375-380.
17. M. C. Thielges and M. D. Fayer, *Accounts of Chemical Research*, 2012, **45**, 1866-1874.
18. H. Ishikawa, S. Kim, K. Kwak, K. Wakasugi and M. D. Fayer, *Proc. Natl. Acad. Sci.*, 2007, **104**, 19309-19314.
19. N. T. Hunt, *Accounts of Chemical Research*, 2024, **57**, 685-692.
20. S. H. Rutherford, M. J. Baker and N. T. Hunt, *The Journal of Chemical Physics*, 2023, **158**, 030901.
21. P. Hamm, M. Lim and R. M. Hochstrasser, *J. Phys. Chem. B*, 1998, **102**, 6123-6138.
22. J. A. Dunbar, E. J. Arthur, A. M. White and K. J. Kubarych, *J. Phys. Chem. B*, 2015, **119**, 6271-6279.
23. B. H. Jones, C. J. Huber and A. M. Massari, *J. Phys. Chem. B*, 2011, **115**, 24813-24822.
24. D. J. Shaw, K. Adamczyk, P. W. J. M. Frederix, N. Simpson, K. Robb, G. M. Greetham, M. Towrie, A. W. Parker, P. A. Hoskisson and N. T. Hunt, *The Journal of Chemical Physics*, 2015, **142**, 212401.
25. A. Biswas and B. S. Mallik, *RSC Adv.*, 2020, **10**, 6658-6670.
26. P.-A. Cazade, H. Tran, T. Bereau, A. K. Das, F. Kläsi, P. Hamm and M. Meuwly, *The Journal of Chemical Physics*, 2015, **142**, 212415.
27. S. M. Kashid, G. Y. Jin, S. Bagchi and Y. S. Kim, *J. Phys. Chem. B*, 2015, **119**, 15334-15343.
28. J. B. Asbury, T. Steinel, C. Stromberg, S. A. Corcelli, C. P. Lawrence, J. L. Skinner and M. D. Fayer, *J. Phys. Chem. A*, 2004, **108**, 1107-1119.
29. E. M. Bruening, J. Schauss, T. Siebert, B. P. Fingerhut and T. Elsaesser, *The Journal of Physical Chemistry Letters*, 2018, **9**, 583-587.
30. M. Yang, Ł. Szyc and T. Elsaesser, *J. Photochem. Photobiol., A*, 2012, **234**, 49-56.
31. L. M. Kiefer and K. J. Kubarych, *J. Phys. Chem. A*, 2015, **119**, 959-965.
32. P. A. Eckert and K. J. Kubarych, *J. Phys. Chem. A*, 2017, **121**, 2896-2902.
33. M. Horch, J. Schoknecht, S. Wrathall, G. Greetham, O. Lenz and N. Hunt, *Chem. Sci.*, 2019, **10**, 8981-8989.
34. S. Kaziannis, J. A. Wright, M. Candelaresi, R. Kania, G. M. Greetham, A. W. Parker, C. J. Pickett and N. T. Hunt, *Phys. Chem. Chem. Phys.*, 2011, **13**, 10295-10305.
35. J. T. King, C. R. Baiz and K. J. Kubarych, *J. Phys. Chem. A*, 2010, **114**, 10590-10604.
36. B. Procacci, S. L. D. Wrathall, A. L. Farmer, D. J. Shaw, G. M. Greetham, A. W. Parker, Y. Rippers, M. Horch, J. M. Lynam and N. T. Hunt, *J. Phys. Chem. B*, 2024, **128**, 1461-1472.
37. S. L. D. Wrathall, B. Procacci, M. Horch, E. Saxton, C. Furlan, J. Walton, Y. Rippers, J. N. Blaza, G. M. Greetham, M. Towrie, A. W. Parker, J. Lynam, A. Parkin and N. T. Hunt, *Phys. Chem. Chem. Phys.*, 2022, **24**, 24767-24783.
38. A. Ghosh, J. S. Ostrander and M. T. Zanni, *Chem. Rev.*, 2017, **117**, 10726-10759.

39. H. S. Chung, Z. Ganim, K. C. Jones and A. Tokmakoff, *Proc. Natl. Acad. Sci.*, 2007, **104**, 14237-14242.
40. Z. Ganim, H. S. Chung, A. W. Smith, L. P. DeFlores, K. C. Jones and A. Tokmakoff, *Accounts of Chemical Research*, 2008, **41**, 432-441.
41. B. Guchhait, Y. Liu, T. Siebert and T. Elsaesser, *Structural Dynamics*, 2015, **3**, 043202.
42. A. T. Krummel and M. T. Zanni, *J. Phys. Chem. B*, 2006, **110**, 13991-14000.
43. M. Yang, Ł. Szyc and T. Elsaesser, *J. Phys. Chem. B*, 2011, **115**, 13093-13100.
44. K. L. Koziol, P. J. M. Johnson, B. Stucki-Buchli, S. A. Waldauer and P. Hamm, *Current Opinion in Structural Biology*, 2015, **34**, 1-6.
45. C. Kolano, J. Helbing, M. Kozinski, W. Sander and P. Hamm, *Nature*, 2006, **444**, 469-472.
46. L. P. DeFlores and A. Tokmakoff, *J. Am. Chem. Soc.*, 2006, **128**, 16520-16521.
47. N. Demirdöven, C. M. Cheatum, H. S. Chung, M. Khalil, J. Knoester and A. Tokmakoff, *J. Am. Chem. Soc.*, 2004, **126**, 7981-7990.
48. L. P. DeFlores, Z. Ganim, R. A. Nicodemus and A. Tokmakoff, *J. Am. Chem. Soc.*, 2009, **131**, 3385-3391.
49. C. R. Baiz, C. S. Peng, M. E. Reppert, K. C. Jones and A. Tokmakoff, *Analyst*, 2012, **137**, 1793-1799.
50. S. D. Moran, A. M. Woys, L. E. Buchanan, E. Bixby, S. M. Decatur and M. T. Zanni, *Proc. Natl. Acad. Sci.*, 2012, **109**, 3329-3334.
51. J. P. Lomont, K. L. Rich, M. Maj, J.-J. Ho, J. S. Ostrander and M. T. Zanni, *J. Phys. Chem. B*, 2018, **122**, 144-153.
52. S. H. Rutherford, G. M. Greetham, A. W. Parker, A. Nordon, M. J. Baker and N. T. Hunt, *The Journal of Chemical Physics*, 2022, **157**, 205102.
53. R. Fritzsch, P. M. Donaldson, G. M. Greetham, M. Towrie, A. W. Parker, M. J. Baker and N. T. Hunt, *Anal. Chem.*, 2018, **90**, 2732-2740.
54. S. Y. Chun, M. K. Son, C. R. Park, C. Lim, H. I. Kim, K. Kwak and M. Cho, *Chem. Sci.*, 2022, **13**, 4482-4489.
55. S. Hume, G. Hithell, Gregory M. Greetham, P. M. Donaldson, M. Towrie, A. W. Parker, M. J. Baker and N. T. Hunt, *Chem. Sci.*, 2019, **10**, 6448-6456.
56. S. H. Rutherford, C. D. M. Hutchison, G. M. Greetham, A. W. Parker, A. Nordon, M. J. Baker and N. T. Hunt, *Anal. Chem.*, 2023, **95**, 17037-17045.
57. S. H. Rutherford, G. M. Greetham, M. Towrie, A. W. Parker, S. Kharratian, T. F. Krauss, A. Nordon, M. J. Baker and N. T. Hunt, *Analyst*, 2022, **147**, 3464-3469.
58. N. B. C. Pfukwa, M. Rautenbach, N. T. Hunt, O. O. Olaoye, V. Kumar, A. W. Parker, L. Minnes and P. H. Neethling, *J. Phys. Chem. B*, 2023, **127**, 3774-3786.
59. J. A. de la Paz, A. Bonvalet and M. Joffre, *Opt. Express*, 2019, **27**, 4140-4146.
60. S.-H. Shim and M. T. Zanni, *Phys. Chem. Chem. Phys.*, 2009, **11**, 748-761.
61. K. M. Farrell, J. S. Ostrander, A. C. Jones, B. R. Yakami, S. S. Dicke, C. T. Middleton, P. Hamm and M. T. Zanni, *Opt. Express*, 2020, **28**, 33584-33602.
62. P. M. Donaldson, G. M. Greetham, C. T. Middleton, B. M. Luther, M. T. Zanni, P. Hamm and A. T. Krummel, *Accounts of Chemical Research*, 2023, **56**, 2062-2071.
63. D. E. Spence, P. N. Kean and W. Sibbett, *Opt. Lett.*, 1991, **16**, 42-44.
64. F. J. Furch, T. Witting, M. Osolodkov, F. Schell, C. P. Schulz and M. J. J Vrakking, *Journal of Physics: Photonics*, 2022, **4**, 032001.
65. B. M. Luther, K. M. Tracy, M. Gerrity, S. Brown and A. T. Krummel, *Opt. Express*, 2016, **24**, 4117-4127.
66. G. M. Greetham, P. M. Donaldson, C. Nation, I. V. Sazanovich, I. P. Clark, D. J. Shaw, A. W. Parker and M. Towrie, *Appl. Spectrosc.*, 2016, **70**, 645-653.

67.   G. Hithell, D. J. Shaw, P. M. Donaldson, G. M. Greetham, M. Towrie, G. A. Burley, A. W. Parker and N. T. Hunt, *J. Phys. Chem. B*, 2016, **120**, 4009-4018.
68.   P. M. Donaldson, G. M. Greetham, D. J. Shaw, A. W. Parker and M. Towrie, *J. Phys. Chem. A*, 2018, **122**, 780-787.
69.   P. Hamm, *The Journal of Chemical Physics*, 2021, **154**, 104201.
70.   P. M. Donaldson, R. F. Howe, A. P. Hawkins, M. Towrie and G. M. Greetham, *The Journal of Chemical Physics*, 2023, **158**, 114201.
71.   S. Hume, G. M. Greetham, P. M. Donaldson, M. Towrie, A. W. Parker, M. J. Baker and N. T. Hunt, *Anal. Chem.*, 2020, **92**, 3463-3469.
72.   S. H. Rutherford, A. Nordon, N. T. Hunt and M. J. Baker, *Chemometrics and Intelligent Laboratory Systems*, 2021, **217**, 104408.
73.   D. Buhrke, Y. Lahav, A. Rao, J. Ruf, I. Schapiro and P. Hamm, *J. Am. Chem. Soc.*, 2023, **145**, 15766-15775.
74.   J. M. Anna, M. J. Nee, C. R. Baiz, R. McCanne and K. J. Kubarych, *JOSA B*, 2010, **27**, 382-393.
75.   M. J. Nee, R. McCanne, K. J. Kubarych and M. Joffre, *Opt. Lett.*, 2007, **32**, 713-715.
76.   E. C. Fulmer, F. Ding, P. Mukherjee and M. T. Zanni, *Physical review letters*, 2005, **94**, 067402.
77.   D. R. Skoff, J. E. Laaser, S. S. Mukherjee, C. T. Middleton and M. T. Zanni, *Chemical physics*, 2013, **422**, 8-15.
78.   Y. Feng, I. Vinogradov and N.-H. Ge, *Opt. Express*, 2017, **25**, 26262-26279.
79.   A. Ghosh, A. L. Serrano, T. A. Oudenhoven, J. S. Ostrander, E. C. Eklund, A. F. Blair and M. T. Zanni, *Opt Lett*, 2016, **41**, 524-527.
80.   S. T. Roberts, J. J. Loparo, K. Ramasesha and A. Tokmakoff, *Optics Communications*, 2011, **284**, 1062-1066.
81.   J. Siliquini and L. Faraone, *Semiconductor science and technology*, 1996, **11**, 1906.
82.   C. R. Baiz, D. Schach and A. Tokmakoff, *Opt. Express*, 2014, **22**, 18724-18735.
83.   J. S. Ostrander, A. L. Serrano, A. Ghosh and M. T. Zanni, *ACS Photonics*, 2016, **3**, 1315-1323.
84.   A. M. Stingel and P. B. Petersen, *The Journal of Chemical Physics*, 2021, **155**, 104202.
85.   W. B. Weeks, C. J. Tainter and L. E. Buchanan, *Biophysical Journal*, 2022, **121**, 1549-1559.
86.   C. Baiz, J. Bredenbeck, M. Cho, T. Jansen, A. Krummel and S. Roberts, *The Journal of Chemical Physics*, 2024, **160**, 010401.
87.   B. Procacci, S. H. Rutherford, G. M. Greetham, M. Towrie, A. W. Parker, C. V. Robinson, C. R. Howle and N. T. Hunt, *Spectrochimica Acta Part A: Molecular and Biomolecular Spectroscopy*, 2021, **249**, 119319 - 119327.
88.   R. Gautam, S. Vanga, F. Ariese and S. Umapathy, *EPJ Techniques and Instrumentation*, 2015, **2**, 1-38.
89.   R. Bloem, S. Garrett-Roe, H. Strzalka, P. Hamm and P. Donaldson, *Opt. Express*, 2010, **18**, 27067-27078.
90.   J. Réhault and J. Helbing, *Opt. Express*, 2012, **20**, 21665-21677.
91.   I. C. Spector, C. M. Olson, C. J. Huber and A. M. Massari, *Opt. Lett.*, 2015, **40**, 1850-1852.
92.   J. G. Seol, H. Kwon, G. Y. Jin, J. Moon, C. Yi and Y. S. Kim, *J. Phys. Chem. A*, 2019, **123**, 10837-10843.
93.   C. Yan, J. Nishida, R. Yuan and M. D. Fayer, *J. Am. Chem. Soc.*, 2016, **138**, 9694-9703.
94.   J. Nishida, A. Tamimi, H. Fei, S. Pullen, S. Ott, S. M. Cohen and M. D. Fayer, *Proc. Natl. Acad. Sci.*, 2014, **111**, 18442-18447.

95. J. H. Hack, J. P. Dombrowski, X. Ma, Y. Chen, N. H. C. Lewis, W. B. Carpenter, C. Li, G. A. Voth, H. H. Kung and A. Tokmakoff, *J. Am. Chem. Soc.*, 2021, **143**, 10203-10213.

96. J. Nishida and M. D. Fayer, *J. Phys. Chem. B*, 2017, **121**, 11880-11890.

97. K. M. Tracy, M. V. Barich, C. L. Carver, B. M. Luther and A. T. Krummel, *The Journal of Physical Chemistry Letters*, 2016, **7**, 4865-4870.

98. G. Giubertoni, F. Caporaletti, R. van Diest and S. Woutersen, *The Journal of Chemical Physics*, 2023, **158**, 124202.

99. C. A. Meza Ramirez, M. Greenop, L. Ashton and I. u. Rehman, *Applied Spectroscopy Reviews*, 2021, **56**, 733-763.

100. S. Ye, K. Zhong, J. Zhang, W. Hu, J. D. Hirst, G. Zhang, S. Mukamel and J. Jiang, *J. Am. Chem. Soc.*, 2020, **142**, 19071-19077.

101. H. Ren, H. Li, Q. Zhang, L. Liang, W. Guo, F. Huang, Y. Luo and J. Jiang, *Fundamental Research*, 2021, **1**, 488-494.

102. H. Ren, Q. Zhang, Z. Wang, G. Zhang, H. Liu, W. Guo, S. Mukamel and J. Jiang, *Proc. Natl. Acad. Sci.*, 2022, **119**, e2202713119.

103. M. Lasalvia, C. Gallo, V. Capozzi and G. Perna, *Applied Sciences*, 2023, **13**, 10325.

104. X. Shao, H. Zhang, Y. Wang, H. Qian, Y. Zhu, B. Dong, F. Xu, N. Chen, S. Liu, J. Pan and W. Xue, *Nanomedicine: Nanotechnology, Biology and Medicine*, 2020, **29**, 102245 - 102252.

105. J. R. Hands, K. M. Dorling, P. Abel, K. M. Ashton, A. Brodbelt, C. Davis, T. Dawson, M. D. Jenkinson, R. W. Lea, C. Walker and M. J. Baker, *J Biophotonics*, 2014, **7**, 189-199.

106. K. Gajjar, J. Trevisan, G. Owens, P. J. Keating, N. J. Wood, H. F. Stringfellow, P. L. Martin-Hirsch and F. L. Martin, *Analyst*, 2013, **138**, 3917-3926.

107. S. H. Rutherford, G. M. Greetham, P. M. Donaldson, M. Towrie, A. W. Parker, M. J. Baker and N. T. Hunt, *Anal. Chem.*, 2021, **93**, 920-927.

108. M. Leeman, J. Choi, S. Hansson, M. U. Storm and L. Nilsson, *Anal. Bioanal. Chem.*, 2018, **410**, 4867-4873.

109. H. W. Schroeder Jr and L. Cavacini, *Journal of allergy and clinical immunology*, 2010, **125**, S41-S52.

110. S. Kharratian, D. Conteduca, B. Procacci, D. J. Shaw, N. T. Hunt and T. F. Krauss, *Chem. Sci.*, 2022, **13**, 12858-12864.

111. Y. LeCun, Y. Bengio and G. Hinton, *nature*, 2015, **521**, 436-444.

112. G. Hinton, L. Deng, D. Yu, G. E. Dahl, A.-r. Mohamed, N. Jaitly, A. Senior, V. Vanhoucke, P. Nguyen and T. N. Sainath, *IEEE Signal processing magazine*, 2012, **29**, 82-97.

113. Y. LeCun, L. Bottou, Y. Bengio and P. Haffner, *Proceedings of the IEEE*, 1998, **86**, 2278-2324.

114. M.-H. Yang, D. J. Kriegman and N. Ahuja, *IEEE Transactions on pattern analysis and machine intelligence*, 2002, **24**, 34-58.

115. A. B. Nassif, I. Shahin, I. Attili, M. Azzeh and K. Shaalan, *IEEE access*, 2019, **7**, 19143-19165.

116. L. Zhang and S. Shao, *Journal of Applied Physics*, 2022, **132**, 1 - 16.

117. H. Chen, O. Engkvist, Y. Wang, M. Olivecrona and T. Blaschke, *Drug discovery today*, 2018, **23**, 1241-1250.

118. J. Westermayr and P. Marquetand, *Chem. Rev.*, 2020, **121**, 9873-9926.

119. I. H. Sarker, *SN Computer Science*, 2021, **2**, 1-21.

120. W. Sauerbrei, P. Royston and H. Binder, *Statistics in medicine*, 2007, **26**, 5512-5528.

121. G. Shafer and V. Vovk, *Journal of Machine Learning Research*, 2008, **9**, 371-421.

122. D. L. Shrestha and D. P. Solomatine, *Neural networks*, 2006, **19**, 225-235.
123. F. Bonnier, G. Brachet, R. Duong, T. Sojinrin, R. Respaud, N. Aubrey, M. J. Baker, H. J. Byrne and I. Chourpa, *Journal of biophotonics*, 2016, **9**, 1085-1097.
124. K. M. Lima, K. B. Gajjar, P. L. Martin-Hirsch and F. L. Martin, *Biotechnology progress*, 2015, **31**, 832-839.
125. V. E. Sitnikova, M. A. Kotkova, T. N. Nosenko, T. N. Kotkova, D. M. Martynova and M. V. Uspenskaya, *Talanta*, 2020, **214**, 1-8.
126. D. K. Medipally, D. Cullen, V. Untereiner, G. D. Sockalingum, A. Maguire, T. N. Q. Nguyen, J. Bryant, E. Noone, S. Bradshaw and M. Finn, *Therapeutic advances in medical oncology*, 2020, **12**, 1-12.
127. D. A. Scott, D. E. Renaud, S. Krishnasamy, P. Meriç, N. Buduneli, Ş. Çetinkalp and K.-Z. Liu, *Diabetology & metabolic syndrome*, 2010, **2**, 1-9.
128. A. Zlotogorski-Hurvitz, B. Z. Dekel, D. Malonek, R. Yahalom and M. Vered, *Journal of cancer research and clinical oncology*, 2019, **145**, 685-694.
129. P. D. Lewis, K. E. Lewis, R. Ghosal, S. Bayliss, A. J. Lloyd, J. Wills, R. Godfrey, P. Kloer and L. A. Mur, *BMC cancer*, 2010, **10**, 1-10.
130. A. Travo, C. Paya, G. Déléris, J. Colin, B. Mortemousque and I. Forfar, *Anal. Bioanal. Chem.*, 2014, **406**, 2367-2376.
131. S. Gok, O. Z. Aydin, Y. S. Sural, F. Zorlu, U. Bayol and F. Severcan, *Journal of biophotonics*, 2016, **9**, 967-975.
132. C. A. Meza Ramirez, M. Greenop, Y. A. Almoshawah, P. L. Martin Hirsch and I. U. Rehman, *Expert Review of Molecular Diagnostics*, 2023, **23**, 375-390.
133. W. Lee, A. T. Lenferink, C. Otto and H. L. Offerhaus, *Journal of raman spectroscopy*, 2020, **51**, 293-300.
134. R. Bro and A. K. Smilde, *Anal. Methods*, 2014, **6**, 2812-2831.
135. J. Liu, M. Osadchy, L. Ashton, M. Foster, C. J. Solomon and S. J. Gibson, *Analyst*, 2017, **142**, 4067-4074.
136. F. Santos, S. Magalhaes, M. C. Henriques, M. Fardilha and A. Nunes, *Current Metabolomics*, 2018, **6**, 103-111.
137. S. Zhang, Y. Qi, S. P. H. Tan, R. Bi and M. Olivo, *Biosensors*, 2023, **13**, 557.
138. I. C. C. Ferreira, E. M. G. Aguiar, A. T. F. Silva, L. L. D. Santos, L. Cardoso-Sousa, T. G. Araújo, D. W. Santos, L. R. Goulart, R. Sabino-Silva and Y. C. P. Maia, *Journal of Oncology*, 2020, **2020**, 4343590.
139. V. Balan, C.-T. Mihai, F.-D. Cojocaru, C.-M. Uritu, G. Dodi, D. Botezat and I. Gardikiotis, *Materials*, 2019, **12**, 2884.
140. L. Minnes, D. J. Shaw, B. P. Cossins, P. M. Donaldson, G. M. Greetham, M. Towrie, A. W. Parker, M. J. Baker, A. J. Henry and R. J. Taylor, *Anal. Chem.*, 2017, **89**, 10898-10906.
141. C. D. Rankine and T. Penfold, *The Journal of Chemical Physics*, 2022, **156**, 164102.
142. J. Zhang, S. Ye, K. Zhong, Y. Zhang, Y. Chong, L. Zhao, H. Zhou, S. Guo, G. Zhang and B. Jiang, *J. Phys. Chem. B*, 2021, **125**, 6171-6178.
143. L. Zhao, J. Zhang, Y. Zhang, S. Ye, G. Zhang, X. Chen, B. Jiang and J. Jiang, *JACS Au*, 2021, **1**, 2377-2384.
144. S. Ye, K. Zhong, Y. Huang, G. Zhang, C. Sun and J. Jiang, *J. Am. Chem. Soc.*, 2024, **146**, 2663-2672.
145. D. Balcells and B. B. Skjelstad, *Journal of chemical information and modeling*, 2020, **60**, 6135-6146.
146. C. D. Rankine and T. J. Penfold, *J. Phys. Chem. A*, 2021, **125**, 4276-4293.
147. A. W. Senior, R. Evans, J. Jumper, J. Kirkpatrick, L. Sifre, T. Green, C. Qin, A. Žídek, A. W. Nelson and A. Bridgland, *Nature*, 2020, **577**, 706-710.

148. D. P. Ismi and R. Pulungan, *Computational and Structural Biotechnology Journal*, 2022, **20**, 6271-6286.
149. M. Candelaresi, E. Ragnoni, C. Cappelli, A. Corozzi, M. Lima, S. Monti, B. Mennucci, F. Nuti, A. M. Papini and P. Foggi, *J. Phys. Chem. B*, 2013, **117**, 14226-14237.
150. J. T. King and K. J. Kubarych, *J. Am. Chem. Soc.*, 2012, **134**, 18705-18712.
151. C. H. Londergan, Y. Sam Kim and R. M. Hochstrasser, *Molecular Physics*, 2005, **103**, 1547-1553.
152. C. S. Peng, K. C. Jones and A. Tokmakoff, *J. Am. Chem. Soc.*, 2011, **133**, 15650-15660.
153. C.-J. Feng, B. Dhayalan and A. Tokmakoff, *Biophysical journal*, 2018, **114**, 2820-2832.
154. H. J. Butler, J. M. Cameron, C. A. Jenkins, G. Hithell, S. Hume, N. T. Hunt and M. J. Baker, *Clinical Spectroscopy*, 2019, **1**, 100003.
155. M. J. Ryan, N. Yang, K. Kwac, K. B. Wilhelm, B. K. Chi, D. J. Weix, M. Cho and M. T. Zanni, *Proc. Natl. Acad. Sci.*, 2023, **120**, e2314998120.
156. N. Yang, M. J. Ryan, M. Son, A. Mavrič and M. T. Zanni, *J. Phys. Chem. B*, 2023, **127**, 2083-2091.
157. Y. El Khoury, L. J. G. W. Van Wilderen and J. Bredenbeck, *The Journal of Chemical Physics*, 2015, **142**, 212416.
158. L. M. Kiefer, L. B. Michocki and K. J. Kubarych, *The Journal of Physical Chemistry Letters*, 2021, **12**, 3712-3717.
159. B. Dereka, N. H. C. Lewis, Y. Zhang, N. T. Hahn, J. H. Keim, S. A. Snyder, E. J. Maginn and A. Tokmakoff, *J. Am. Chem. Soc.*, 2022, **144**, 8591-8604.
160. Y. Wang and D. Chen, *ACS Applied Materials & Interfaces*, 2022, **14**, 23033-23055.
161. P. Garrett and C. R. Baiz, *Soft Matter*, 2022, **18**, 1793-1800.
162. S. A. Roget, Z. A. Piskulich, W. H. Thompson and M. D. Fayer, *J. Am. Chem. Soc.*, 2021, **143**, 14855-14868.
163. K. M. Slenkamp, M. S. Lynch, B. E. Van Kuiken, J. F. Brookes, C. C. Bannan, S. L. Daifuku and M. Khalil, *The Journal of Chemical Physics*, 2014, **140**, 084505.
164. R. Fernández-Terán, J. Ruf and P. Hamm, *Inorganic Chemistry*, 2020, **59**, 7721-7726.
165. B. Procacci, S. L. Wrathall, A. L. Farmer, D. J. Shaw, G. M. Greetham, A. W. Parker, Y. Rippers, M. Horch, J. M. Lynam and N. T. Hunt, *J. Phys. Chem. B*, 2024, **128**, 1461–1472.
166. X. Dong, P. Yu, J. Zhao, Y. Wu, M. Ali, M. A. El-Sayed and J. Wang, *J. Phys. Chem. B*, 2023, **127**, 3532-3541.